Single-cell RNA-Sequencing uncovers transcriptional states and fate decisions in haematopoiesis

Emmanouil I. Athanasiadis[1-3,*], Jan G. Botthof[1-3,*], Helena Andres[4], Lauren Ferreira[1-3,5], Pietro Lio[4], Ana Cvejic[1-3]

[1] Department of Haematology, University of Cambridge, Cambridge, CB2 0XY, UK

[2] Wellcome Trust Sanger Institute, Wellcome Trust Genome Campus, Cambridge, CB10 1SA, UK

[3] Wellcome Trust – Medical Research Council Cambridge Stem Cell Institute, Cambridge, CB2 1QR, UK

[4] Computer Laboratory, University of Cambridge, Cambridge, CB3 0FD, UK

[5] Current address: Biotechnology Innovation Centre, Rhodes University, Grahamstown, 6139, South Africa

Correspondence: Ana Cvejic, Wellcome Trust Sanger Institute, Wellcome Genome Campus, The Morgan Building, Hinxton, Cambridge, Cambridgeshire, CB10 1SA.
E-mail: as889@cam.ac.uk

*E.I.A and J.G.B contributed equally to this study

ABSTRACT

The success of marker-based approaches for dissecting haematopoiesis in mouse and human is reliant on the presence of well-defined cell-surface markers specific for diverse progenitor populations. An inherent problem with this approach is that the presence of specific cell surface markers does not directly reflect the transcriptional state of a cell. Here we used a marker-free approach to computationally reconstruct the blood lineage tree in zebrafish and order cells along their differentiation trajectory, based on their global transcriptional differences. Within the population of transcriptionally similar stem and progenitor cells our analysis revealed considerable cell-to-cell differences in their probability to transition to another, committed state. Once fate decision was executed, the suppression of transcription of ribosomal genes and up-regulation of lineage specific factors coordinately controlled lineage differentiation. Evolutionary analysis further demonstrated that this haematopoietic program was highly conserved between zebrafish and higher vertebrates.

INTRODUCTION

Mammalian blood formation is the most intensely studied system of stem cell biology, with the ultimate aim to obtain a comprehensive understanding of the molecular mechanisms controlling fate-determining events. A single cell type, the haematopoietic stem cell (HSC), is responsible for generating more than 10 different blood cell types throughout the lifetime of an organism[1]. This diversity in the lineage output of HSCs is traditionally presented as a stepwise progression of distinct, transcriptionally homogeneous populations of cells along a hierarchical differentiation tree[2–6]. However, most of the data used to explain the molecular basis of lineage differentiation and commitment were derived from populations of cells isolated based on well-defined cell surface markers[7]. One drawback of this approach is that a limited number of markers is used simultaneously to define the blood cell identity. Consequently, only a subpopulation of the overall cellular pool is examined and isolated cells, although homogeneous for the selected markers, show considerable transcriptional and functional heterogeneity[8–12]. This led to the development of various refined sorting strategies in which new combinations of marker genes were considered to better "match" the transcriptional and functional properties of the cells of interest.

The traditional model of haematopoiesis assumes a stepwise set of binary choices with early and irreversible segregation of lymphoid and myeloid differentiation pathways[2,3]. However, the identification of lymphoid-primed multipotent progenitors (LMPP)[4], which have granulocytic, monocytic and lymphoid potential but low potential to form megakaryocyte and erythroid lineages prompted development of alternative models of haematopoiesis. More recently, it has been demonstrated that megakaryocyte-erythroid progenitors can progress directly from HSC without going through a common myeloid intermediate (CMP)[13]; or that the stem cell compartment is multipotent, while the progenitors are unipotent[6]. Clear consensus on the lineage branching map, however, is still lacking.

Recent advances in single-cell transcriptional methods have made it possible to investigate cellular states and their transitions during differentiation, allowing elucidation of cell fate decision mechanisms in greater detail. Computational ordering methods have proved to be particularly useful in reconstructing the differentiation process based on the transcriptional changes of cells at different stages of lineage progression[14–16].

Here we created a comprehensive atlas of single cell gene expression in adult zebrafish blood cells and computationally reconstructed the blood lineage tree *in vivo*. Conceptually, our approach differs from the marker based method in that the identity of the cell type/state is determined in an unbiased way i.e. without prior knowledge of surface markers. The

transcriptome of each cell was projected on the reconstructed differentiation path giving complete insight into the cell state transitions occurring during blood differentiation. Importantly, development of this strategy allowed us, for the first time, to asses haematopoiesis in a vertebrate species in which surface marker genes/antibodies are not readily available. Finally, this study provides unique insight into the regulation of haematopoiesis in zebrafish and also, along with complementary data from mouse and human, addresses the question of interspecies similarities of haematopoiesis in vertebrates.

RESULTS

Single cell RNA-Sequencing analysis of 1,422 zebrafish haematopoietic cells

As an alternative to marker-based cellular dissection of haematopoietic hierarchy, we have set out to classify haematopoietic cells based on their unique transcriptional state. We started by combining FACS index sorting with single cell RNA-Seq to reveal the cellular properties and gene expression of a large number of blood cells simultaneously. To cover the entire differentiation continuum, kidney derived blood cells from eight different zebrafish transgenic reporter lines and one non-transgenic line were FACS sorted (Fig. 1a, Supplementary Table 1). Each blood cell was collected in a single well of a 96-well plate. At the same time, information about the cell size (FSC) and granularity (SSC), as well as the level of the fluorescence, were recorded.

RNA from each cell was isolated and used to construct a single mRNA-Seq library per cell, which was then sequenced to a depth of around $1x10^6$ reads per library. Following quality control (QC) 1,422 cells were used for further analysis and for benchmarking of different alignment methods (Supplementary Fig. 1, 2 and 3). Importantly, the average single-cell profiles showed good correlation with independent bulk samples (PCC=0.7-0.9, Supplementary Fig. 3e). In addition, PCA, ICA and Diffusion maps (Supplementary Fig. 4a) showed that cells were intermixed irrespective of the fish or the plate they originated from. This confirmed that the cells were separated in the analyses based on their biological differences rather than batch induced biases.

HSPC can reach specific cell fates through a single path in the “state-space”

A dynamic repertoire of gene expression in thousands of cells during differentiation could be used to infer a single branched differentiation trajectory. Due to the unsynchronised nature of haematopoiesis each single cell exhibits a different degree of differentiation along the differentiation continuum. Therefore, the generated trajectory could be used to infer the differentiation path of a single cell. To examine the transcriptional transition undergone by

differentiating cells, we identified the 1,845 most highly variable genes (Supplementary Fig. 4b) and performed expression based ordering using Monocle2[15]. Based on global gene expression profiles of the cells, we identified five (1-5) distinct cell "states" (Fig. 1b). To ensure the robustness of this approach, we verified computationally that changes in the highly variable genes and Monocle2 settings only lead to minor differences in the trajectory, mainly around the branching points (Supplementary Fig. 5).

Differential expression analysis of each state versus all other states, followed by gene ontology (GO) enrichment analysis (see methods), provided clear insights into the cell types in each state (Fig. 1c). Specifically, state 1 contains GO terms relating to antigen processing, including genes that are highly expressed in the monocyte lineage, such as *cd74a/b*[17], *ctss2.2*[18] and *mhc2dab*[19] (Supplementary Table 2). The functionality of state 2 relates to leukocyte migration, including genes specific to neutrophils (e.g. *cxcr4b*[20], *rac2*[21] and *wasb*[22,23] (Supplementary Table 2). State 3 is highly enriched for genes that are involved in ribosome biogenesis, including *fbl* (Fibrillarin) and *pes* (Pescadilo), both of which are critical for stem cell survival[24,25] (Supplementary Table 2). Since there is also enrichment for HSC homeostasis, this state is most likely to be haematopoietic stem/progenitor cells (HSPCs). With GO terms that include gas exchange and erythrocyte differentiation involving the adult haemoglobins, *ba1*, *ba1l* and *hbaa1*[26] together with the erythroid-specific aquaporin gene, *aqp1a*[26,27] (Supplementary Table 2), state 4 can be assigned to the erythroid lineage. Finally, state 5 has functionality that is relevant for circulatory system development and blood coagulation, both of which include *itga2b* (also known as *cd41*) together with its heterodimer *itgb3b*[28] (Supplementary Table 2). Since these gene lists include other genes that interact with this platelet integrin receptor complex, as well as additional genes relevant for platelet function, we assigned this cell state to thrombocytes. Mature lymphocytes could not be detected, most likely as T-cells mature in the thymus and B-cells are comparatively rare and were not enriched for.

To experimentally confirm our computational predictions, we sorted cells from transgenic lines that were the most abundant in each of the five states (Fig. 2) and stained them using May-Grünwald Giemsa staining. Indeed, the morphological properties of the sorted cells (Fig. 1c, Supplementary Fig. 6-7) matched the assigned cell types, therefore adding confidence to these cell type assignations. As expected, the signature genes such as *marco*, *lyzC*, *hhex*, *alas2* and *itga2b* were within the most differentially expressed genes in monocytes, neutrophils, HSPC, erythrocytes and thrombocytes respectively (Fig. 1d).

Taken together, the reconstructed branched tree revealed a gradual transition of myeloid cells from immature to more differentiated cells. Within this tree, HSPCs assumed a new committed state through a single path, suggesting that during steady state haematopoiesis, HSPCs can reach a specific cell fate through only one type of intermediate progenitor.

Cells within distinct states differ in their repopulation potential

Functional *in vivo* transplantation assays have been traditionally used to assess the differentiation potential of different haematopoietic populations. To examine the repopulation and lineage potential of the cells within different states we sorted cells from *Tg(mpx:EGFP)*[29], *Tg(gata1:EGFP)*[30] and *Tg(runx1:mCherry)*[31] fish to enrich for neutrophil, erythroid and HSPC cell state respectively. We next injected 500 donor cells into sub-lethally irradiated, immunocompromised *rag2*$^{E450fs-/-}$ zebrafish[32] and assessed their engraftment at one day, four- and fourteen weeks post injection (PI) (Fig. 3a).

Analysis of kidney repopulation revealed that *mpx*+, *gata1*+ and *runx1*+ cells were able to home to the kidney one day PI (Fig. 3b). However, only progeny of *runx1*+ cells were detectable at four weeks PI in all examined recipients (Fig. 3b). No progeny of *mpx*+ and *gata1*+ cells were evident at the same time point. To examine the lineage output of *runx1*+ cells following transplantation we sorted engrafted *runx1*+ kidney cells four and 14 weeks PI and processed them for scRNA-Seq analysis. The scRNA-Seq data from 302 engrafted *runx1*+ cells projected onto a Monocle trajectory revealed the multilineage potential of donor *runx1* cells at both four and fourteen weeks PI (Fig. 3c). These data strongly suggested that at least some of these cells were HSCs.

According to transplantation assays, cytospins and transcriptional profiling of cells prior and following transplantation, cells located in the branches of the Monocle tree show progression of lineage restricted progenitors to mature blood cells with no repopulation potential. However, cells in the middle of the Monocle tree (state 3) are a mixture of progenitors and HSCs with long term multilineage potential.

Resolving the heterogeneity within the HSPC branch of the lineage tree

To increase the number of HSCs in our data set and the resolution in the HSPC branch of the Monocle trajectory, we added the 302 transplanted *runx1*+ cells to our 1,422 previously sequenced cells. We re-analysed the whole data set (1,724 cells in total), and generated a new Monocle trajectory (Fig. 4a).

Next, we considered the frequency of potential HSCs in this data set. To do so, we computed the stemness S^{rel} index[33], using the Kullback–Leibler distance of the predicted probabilities compared to the expected one, for each of the four different branches (Fig. 4a and b). The lower the "stemness" factor, the higher the confidence that a particular cell is a stem cell. Using the threshold of 3 sigma over the mean stemness value (0.05), our analysis predicted that 35 out of 214 cells in the middle part of the tree are potential HSCs. The majority of cells that were identified as stem cells originated from the *cd41* (13 cells) and *runx1* (14 cells) transgenic lines (Fig. 4c). It should be noted that both these lines have been previously identified to contain transplantable HSCs[31,34], lending further confidence to our computational prediction. This suggests that, although both stem and progenitor cells are intermixed on the trajectory due to their overall similar transcriptomes, their lineage potentials (and thus stemness scores) are distinct.

Suppression of transcription of ribosomal genes and up-regulation of lineage specific factors coordinately control lineage differentiation

Differentiation generally involves specific regulated changes in gene expression. To understand the dynamics of transcriptional changes during the differentiation of myeloid cells, we examined trends in gene expression in each of the four branches (Fig. 5). Dynamically expressed genes within each of the branches showed two main trends (see methods). These included genes gradually upregulated through pseudotime and genes gradually downregulated (Fig. 5a-b).

Genes upregulated in pseudotime included well known genes related to the specific function of the relevant cell type (Fig. 5b). The majority of cells characterised as erythroid dynamically expressed genes such as *alas2, aqp1a.1, ba1*, *ba1l*, *cahz* and *hbaa1*. Similarly, cells in the monocyte branch dynamically expressed genes like *c1qa*, *cd74a*, *ifngr1*, *marco*, *myod1* and *spi1a*; among other genes the *cebpb*, *cfl1*, *cxcr4b*, *illr4*, *mpx* and *ncf1* were upregulated in pseudotime in the neutrophil branch and thrombocytes dynamically expressed *fn1b*, *gp1bb*, *itga2b*, *mpl*, *pbx1a* and *thbs1b*. A complete list of all genes that were dynamically expressed across pseudotime can be found in Supplementary Table 2.

Interestingly, genes downregulated through pseudotime (Fig. 5b) in each of the four branches were consistently enriched for genes involved in ribosome biosynthesis, as revealed by GO terms "biosynthetic process", "ribosome" and "translation" (Supplementary Table 2). This is an interesting finding, because previous studies suggested that HSCs have significantly lower rates of protein synthesis than other haematopoietic cells[35]. Therefore, we

went on to investigate the expression of ribosomal proteins in pseudotime in greater depth (Fig. 5c).

Out of 168 genes annotated as “ribosomal proteins” on Ensembl BioMart database (Supplementary Table 2), 89 genes had low, random expression in our dataset (Fig. 5c). These genes encoded mainly mitochondrial ribosomal proteins (Fig. 5c). In contrast, 79 genes that showed high expression across all cells encoded cytoplasmic ribosomal proteins and were downregulated in pseudotime in all four branches (Fig 5c). Importantly, the observed downregulation of ribosomal genes in pseudotime was not correlated with the cell cycle state of the cell, apart from a weak correlation in the erythrocytic lineage (Supplementary Fig. 8). These findings further indicate that there is a common developmental event in which suppression of transcription of ribosomal genes and up-regulation of lineage specific factors direct lineage commitment and terminal differentiation.

A previous study showed that the rate of protein synthesis in murine HSCs is considerably lower than that of progenitor populations (i.e. CMPs, GMPs and MEPs)[35]. This is not in line with our transcriptional analysis, which showed a decrease in ribosomal gene expression during differentiation. In order to address this discrepancy, we considered the correlation in ribosomal gene expression between human phenotypic HSCs (CD34+ CD38- CD45RA- CD90+ CD49f+) and the different progenitor fractions (for details please see Methods). We used a publicly available scRNA-Seq data set from bone marrow derived HSPCs and analysed the expression of genes that encode cytosolic ribosomal proteins. After calculating average $\log_{10}$ expression profiles for each of the six different cell types (HSC, MPP, MLP, CMP, GMP and MEP), we calculated the pairwise Pearson correlation. The analysis revealed very strong correlations (0.92-0.99) between the the ribosomal gene expression in HSCs and all five progenitor populations (Supplementary Fig. 9). Therefore, even though HSCs have 10-fold higher de novo protein synthesis[35], their level of expression of genes that encode ribosomal proteins is similar (highly correlated) to that of the progenitor populations. Our results described above suggested that there is a poor correlation between the level of transcription of ribosomal genes and *de novo* protein synthesis. As this was observed in both human and zebrafish cells, it is likely that the lack of correlation has been evolutionarily conserved.

Zebrafish have a highly conserved HSPC transcriptome compared to mouse and human

Zebrafish are an important model system in biomedical research and has been extensively used for the study of haematopoiesis. Although it has been demonstrated that many

transcription factors and signaling molecules in haematopoiesis are well conserved between zebrafish and mammals[36], comparative analysis of the whole transcriptome was lacking.

In order to explore the evolution of blood cell type specific genes, we performed conservation analysis between zebrafish and other vertebrate species (see Methods). For this analysis, we enriched our initial dataset with 81 natural killer (NK) and 109 T-cells derived from the spleen of two adult zebrafish[37]. Our analysis revealed particularly high conservation of the HSPC transcriptome. For example, 90% of HSPC specific genes in zebrafish had an ortholog in human and mouse compared to 70-80% of erythrocyte-, monocyte-, neutrophil- and thrombocyte-specific genes (Fig. 6a). The lowest conservation was observed for T-cells (59%) and NK cells (68%), possibly reflecting their adaptation to fish specific pathogens and virulence factors (Fig. 6a).

Gene duplication is the major process of gene divergence during the molecular evolution of species[38]. We therefore analysed duplications that occurred exclusively before (referenced hereafter as pre-speciation genes) or after speciation (referenced hereafter as post-speciation genes) of the last common ancestor between fish (Actinopterygii) and mammals (Sarcopterygii)[37,39], (see methods section). Out of 7,424 paralogs that were expressed in our data set (see Methods) around 79% were duplicated pre- and 21% were duplicated post-speciation (Fig. 6b). Following ray-finned specific duplication, the paralogs were more likely to functionally diverge (88%) and show expression in different cell types than to remain expressed in the same cell type (conserved expression), 12% (Fig. 6b and c). Interestingly, HSPCs had the highest percentage of paralogs (19%) with a conserved expression pattern (Fig. 6c). This number was lowest for duplicated genes in innate (0% for the neutrophils and 6% in monocytes) and adaptive immune cells (8% for the NK and 6% for the T-cells). Altogether our findings further underline the relevance of the zebrafish model system in advancing our understanding of the genetic regulation of haematopoiesis in both normal and pathological states.

BASiCz - Blood Atlas of Single Cells in zebrafish

The characterisation of mouse and human haematopoietic cells is dependent on the presence of cell-surface markers and availability of antibodies specific for diverse progenitor populations. The antibodies for these cell surface markers are thus used to isolate relatively homogeneous cell populations by flow cytometry. Transcriptional profiling of isolated cell populations[40–42] and more recently single cells[43], have further allowed genome-wide identification of cell-type specific genes. However, beyond mouse and human, less is known about the transcriptome of blood cell types, mainly due to the lack of suitable antibodies.

To overcome this knowledge gap, we have generated a user-friendly cloud repository, BASiCz (Blood Atlas of Single Cells in zebrafish) for interactive exploration and visualisation of 31,953 zebrafish genes in 1,422 haematopoietic cells across five different cell types. The generated database (http://www.sanger.ac.uk/science/tools/basicz) allows easy access and retrieval of sequencing data from zebrafish blood cells.

DISCUSSION

Cell differentiation during normal blood formation is considered to be an irreversible process with a clear directionality of progression from HSCs to more than 10 different blood cell types. It is, however, widely debated to what extent the process is gradual or direct[6,13] on the cellular level; and in the case of the gradual model, what the intermediates of the increasingly restricted differentiation output of progenitor cells are[2–5,33]. Although these models are very different in the way that they describe lineage progression, the identity of haematopoietic cells is determined based on the cell surface markers and the progression of cells during differentiation is defined on a cellular rather than transcriptional level.

Here we used a marker free approach to order cells along their differentiation trajectory based on the transcriptional changes detected in the single cell RNA-Seq dataset. Our analysis showed a gradual transition of cells on a global transcriptional level from multipotent to lineage restricted. The computationally reconstructed tree further revealed that differentiating cells moved along a single path in the “state-space”. This path included an early split of cells towards thrombocyte-erythrocyte and monocyte-neutrophil trajectories. However, cells in the “middle” of the tree (HSPC state) showed considerable cell-to-cell variability in their probability to transition to any of the four cell types. This suggested that although global transcriptional changes before and after the branching point were continuous, the probability of a cell transitioning to any of the four committed states was determined only by a subset of highly relevant genes. Therefore, cells that were transcriptionally similar overall could have a high probability of differentiation to distinct cell types.

Interestingly, once the cell fate decision was executed, suppression of transcription of ribosomal genes and up-regulation of genes which are relevant for the function of each cell type coordinately controlled lineage differentiation. Of all genes that were annotated as “ribosomal proteins” on the Ensembl BioMart database, only those that encoded cytoplasmic ribosomal proteins showed dynamic expression in pseudotime in our dataset. Importantly, this change was not linked to the expression of cell cycle specific genes, excluding

proliferation rates as a potential reason for these data. These findings are not in line with previous studies, which suggested that HSCs have significantly lower rates of protein synthesis compared to other haematopoietic cells. It should be noted, however, that in this study we measured the transcription of genes that encoded ribosomal proteins rather than *de novo* protein synthesis like in[35]. Furthermore, our analysis of data obtained from human HSCs and progenitors revealed that ribosomal gene expression levels are highly similar between the different progenitor types and stem cells, despite their significantly different protein synthesis rates[35]. Thus, one plausible explanation for the observed discrepancies is a low correlation between transcription of the ribosomal genes and protein production and that these two processes are to some extent uncoupled during blood differentiation.

Our comparative analysis between zebrafish, mouse and human across seven different haematopoietic cell types revealed a high overall conservation of blood cell type specific genes. Together with BASiCz, a user-friendly cloud repository, we generated a comprehensive atlas of single-cell gene expression in adult zebrafish blood. Data-driven classification of cell types provided high-resolution transcriptional maps of cellular states during differentiation. This allowed us to define the haematopoietic lineage branching map, for the first time, in zebrafish *in vivo*.

METHODS

Zebrafish Strains and Maintenance

The maintenance of wild-type (Tubingen Long Fin) and transgenic zebrafish lines[29–31,44–48] (Supplementary Table 1) was performed in accordance with EU regulations on laboratory animals, as previously described[49].

Single-Cell Sorting

A single kidney from heterozygote transgenic or wild-type fish was dissected and placed in ice cold PBS/5% fetal bovine serum. At the same time, testes were dissected from the same fish. Single cell suspensions were generated by first passing through a 40 µm strainer using the plunger of a 1 ml syringe as a pestle. These were then passed through a 20 µm strainer before adding 4',6-diamidino-2-phenylindole (DAPI, Beckman Coulter, cat no B30437) for *mCherry/dsRed2*, or propidium iodide (PI, Sigma cat no P4864) for *GFP/EGFP*. Individual cells were index sorted into wells of a 96 well plate using a BD Influx Index Sorter. Kidneys from a non-transgenic line were used as a control for gating[16].

Whole Transcriptome Amplification

The Smart-seq2 protocol[50,51] was used for whole transcriptome amplification and library preparation as described previously[16] using 92 External RNA Controls Consortium (ERCC) spike-ins[52] at a final dilution of 1:10. These were sequenced on the Illumina Hi-Seq2500 or Hi-Seq4000 platforms.

Cytology

Sorted transgene-positive or gated wild type cells were concentrated by cytocentrifugation at 350 rpm for 5 minutes onto SuperFrostPlus slides using a Shandon Cytospin 3 cytocentrifuge. Slides were fixed for 3 minutes in -20°C methanol and stained with May-Grünwald Giemsa (Sigma) as described elsewhere[53]. Images were captured as described elsewhere[49].

Transplantation experiments

Adult *rag2*$^{E450fs-/-}$ mutant fish[32] were irradiated in an IBL 437 irradiator using a 10 Gy dose from a Caesium 137 source. After 1-2 days of recovery, donor cells were prepared from kidneys of transgenic fish as described above. Using the same gating strategy as employed for the single cell sorting, fluorescent cells were collected by flow cytometry into microtubes containing 20 µl ice cold PBS/5% fetal bovine serum. Using a volume of 10 µl, 500 cells were transplanted into the anaesthetised (0.02% tricaine, Sigma A5040) *rag2*$^{E450fs-/-}$ recipients via intraperitoneal injection. As described above, engraftment into the whole kidney marrow was analysed by FACS at one day, four- and fourteen weeks post transplantation. The engrafted cells at four and fourteen weeks post transplantation were single cell index sorted and processed for single cell RNA-Seq as described above.

Benchmarking single-cell RNA sequencing methods

One of the most important components that contributes to errors during the alignment and quantification of single-cell RNA-Sequencing data is the presence of multi-mapped (or ambiguous) reads[54]. Currently, there are many different bioinformatic strategies that can be used to align (e.g. STAR[55], Tophat[56], Bowtie[57], Salmon[58], Sailfish[59], Kallisto[60] etc.) and quantify scRNA-seq data (e.g. htseq[61], cufflinks[62], Salmon[58], Sailfish[59], Kallisto).

However, independent of the method applied, one of two possible strategies can be used to align reads, namely unique and multi-mapped. A comprehensive comparative analysis across many different scRNA-seq approaches has recently been published. It suggests that both setups (i.e. single and multi-mapped reads) are able to cope with ambiguous reads effectively[54].

In order to assess the impact of using a unique versus multi-mapped reads alignment strategy on our data set, we re-analysed our raw data using STAR[55] in uniquely aligned reads mode. Salmon[58] was used next to quantify the transcripts. The Pearson correlation of the average gene expressions between Salmon and Sailfish at single cell level ranged from 0.81 to 0.91, suggesting a strong correlation between alignments that included uniquely-mapped reads and those that did not (Supplementary Fig. 1a). As expected, the number of detected genes (TPM > 1) was lower for Salmon compared to Sailfish (Supplementary Fig. 1b). However, the genes' variability distribution (Coefficient of Variation CV) across single cells for each plate was comparable between the two methods (Supplementary Fig. 1c).

Extended analysis of the reconstructed lineage tree in zebrafish

To further investigate how robust our computational reconstruction of the lineage tree is, we applied different cutoffs to define variable genes. We next reconstructed the lineage tree using Monocle2[15]. Specifically, the highly variable genes were calculated using: 5% biological variation, 25%- (default analysis) and 95% biological variation (three components). We then analysed the overall structure of the tree and the percentage of the misclassified cells as compared to the default setting that we used in the initial submission.

Single cell RNAseq processing and Quality Control

Reads were aligned to the zebrafish reference genome (Ensemble BioMart version 83) combined with the *EGFP*, *mCherry*, *tdTomato* and ERCC spike-ins sequences. Quantification was performed using Sailfish[59] version 0.9.0 with the default parameters using paired-end mode (parameter –l IU).

Transcript Per Million (TPM) values reported by Sailfish were used for the quality control (QC) of the samples. Wells with fewer than 1,000 expressed genes (TPM>1), or more than 60% of ERCC or Mitochondrial content were initially annotated as poor quality cells (Supplementary Fig. 1). However, due to the lower number of expressed genes in erythroid cells, we further investigated the expression levels of adult globin genes, *ba1* and *hbaa1*[26], in all erythroid cells. Based on comparison with the empty wells, samples that expressed both *ba1* (> 40,000 TPM) and *hbaa1* (> 9000 TPM) were considered to pass QC (Supplementary Fig. 2). Therefore, a total of 1,422 single cells were selected for further analysis.

Average single-cell profiles compared to corresponding bulk wells revealed strong correlations (Pearson's Correlation Coefficient) ranging from 0.7 to 0.9 as illustrated in

Supplementary Fig. 2, suggesting that the single cell expression profiles were effectively quantified.

For each of the 1,422 single cells, both gene and ERCC counts reported by Sailfish, were transformed into normalised counts per million (CPM). To do this, we divided the number of counts for each gene by the total number of counts (i.e. sum of all counts per cell) in each cell followed by multiplication of the resulting number by 1,000,000. The library size and cell-specific biases were removed (e.g. differences during amplification, ERCC concentration, batch effects etc.) using the scran R package (version 1.3.0)[63]. Out of 31,953 genes, we retained those that were expressed in at least 1% of all cells (CPM>1). Thus, a total of 20,960 genes were used for further analysis.

Technical noise fit and identification of highly variable genes

To distinguish biological variability from the technical noise in our single-cell experiments we inferred the most highly variable genes using ERCCs as spike-in in all 1,422 blood cells[64]. We used the scLVM[65] R package (version 0.99.2) to identify the 1,845 most highly variable genes (Supplementary Fig. 3).

Principal Component Analysis (pcaMethods[66] (version 1.64.0)), Independent Component Analysis (FastICA[67] (version 1.2) and Diffusion Maps (destiny[68] (version 1.3.4)), were used to verify that all cells were intermixed in the reconstructed 3D component space based on their transcriptional properties and not based on the fish or a plate they originated from.

Pseudotime ordering of zebrafish haematopoietic cell, differential expression analysis and the analysis of dynamically expressed genes

The set of 1,845 most highly variable genes was used to order the 1,422 single cells along a trajectory using the Monocle2[15] R package (version 1.99.0). The “tobit” expression family and “DDRTree” reduction method were used with the default parameters. As illustrated in Fig. 1, cells ordered in the pseudotime created five distinct states. To assign identity to each of the five states, we performed differential expression (DE) analysis between each state versus the remaining four using the “differentialGeneTest” Monocle2 function. We modeled expression profiles of each state using a Tobit family generalized linear model (GLM) as described previously[15]. For each state, statistically significant genes that scored $P < 0.01$, $q < 0.1$ (False Discovery Rate) and were expressed in more than 50% of the cells were further used to perform Gene Ontology (GO) analysis.

To enrich for HSPCs, we added 302 transplanted *runx1*+ cells to our previous data set for a total of 1,724 cells. We re-analysed the data the same way as described above and used the 1,871 most variable genes for the calculation of a new Monocle trajectory.

Finally, we identified genes that change as a function of pseudotime across each of the four branches by setting the "fullModelFormulaStr" parameter equal to "~sm.ns(Pseudotime)". Genes whose expression changed dynamically in pseudotime were selected using the same statistical criteria as described for DE genes. For each branch we clustered dynamically expressed genes using the "plot_pseudotime_heatmap" function with the default parameters. The number of clusters (trends) in each branch was determined by its silhouette plot score (cluster R package version 2.0.5)[69]. To generate the trend lines across different states (see Fig. 3b), we used the average expression pattern of the dynamically expressed genes that follow the same trend across pseudotime and fit them using *ggplot2*[70] R package (version 2.2.1) *stat_smooth*() parameter. We used the Gaussian linear model and formula the "*y ~ poly(x,2)*" at 0.95 of standard error (gray area of the plot).

For the analysis of ribosomal genes, we used the Ensembl BioMart version 83 and selected all genes annotated with the term "ribosomal protein". We performed clustering using the pheatmap function (R pheatmap package version 1.0.8)[71] using Euclidean distance and ward.D2 linkage.

To investigate the correlation between ribosomal and cell cycle gene expression, we identified a total of 342 zebrafish genes annotated as "GO:0007049" i.e. "cell cycle" using BioMart (version 83). Next, we performed clustering between a subset of the cell cycle genes expressed in more than 10% of cells in each of the branches of the Monocle trajectory and dynamically expressed ribosomal genes using the tools described above.

Analysis of human cells

In order to show the generalisability of our findings from zebrafish to humans, we used a publicly available human single-cell RNA-Seq data set[33] (deposited in the Gene Expression Omnibus (GEO) under accession code GSE75478. This set contained data from 1,344 single cells, which we aligned to the latest human reference genome (GRCh38p10 version 88) and quantified gene expression using Sailfish (version : 0.9.0). Following quality control, we were left with 891 single cells, which included HSCs and various progenitor fractions (Supplementary Table 3). We next identified 341 genes that were annotated as "Ribosomal" using the BioMart database (GRCh38p10 version 88) and were expressed in more than 1% of all cells. Of these, 250 were expressed at a very low level in this data set (add cut off to

define this). GO term enrichment analysis revealed that these genes encode mitochondrial ribosomes. In contrast, 91 genes that were expressed at a high level, encoded cytosolic ribosomal genes, as suggested by GO term enrichment analysis. Since our initial analysis using zebrafish cells focused only on genes that encode cytosolic ribosomes, we focused on the same population of genes in the human data set. Finally, we calculated the pairwise Pearson correlation between the cytosolic ribosomal genes for each progenitor population.

Gene Ontology (GO) analysis

DE genes were ranked for each of the five states based on the mean $\log_{10}$ counts. Genes with average lower than 2 and those expressed in more than one state were not included in the GO analysis. GO analysis was performed using the gProfileR[72] package (Version 0.6.1) using the gprofiler command with the following parameters: organism = 'drerio', hier_filtering ='moderate', correction_method='fdr' and max_p_value = 0.05.

Conservation analysis of the cell type specific genes in zebrafish

In order to perform the conservation analysis, we identified the orthologous genes (BioMart Ensembl Version 83) between the zebrafish and other vertebrate species, including cave fish, tilapia, amazon molly, tetraodon, fugu, cod, human, chimpanzee, mouse, rat, dolphin, wallaby, chicken, lizard, *Xenopus*, coelacanth and lamprey. For this analysis, we enriched our initial dataset with 81 natural killer (NK) and 109 T-cells derived from the spleen of two adult zebrafish[37]. Following the same computational approach as we did with the initial dataset, we re-calculated the DE genes for each of the seven different clusters. We only considered "protein_coding" genes that were expressed in more than 50% of cells within each cluster and scored more than mean $\log_{10}$ counts. This resulted in 41 erythrocyte-, 113 monocyte-, 102 neutrophil-, 212 thrombocyte-, 60 HSPC-, 34 NK- and 34 T- specific genes that were used for the further analysis. For the case of the non-DE genes, we included only "protein_coding" annotated genes that were expressed in more than 1% of all cells (CPM>1) and with average gene expression higher than the global mean of 0.10. The final list of the non-DE genes included 8,127 genes.

Analysis of duplicated genes in zebrafish

In order to analyse duplicated genes[37], we first identified all zebrafish "protein_coding" paralog genes listed in Ensembl (BioMart Ensembl Version 83) and split them into two groups: 1) 17,158 pre ray-finned fish duplicated genes, including *Euteleostomi*, *Bilateria*, *Chordata*, *Vertebrata* and *Opisthokonta* parent taxa, and 2) 11,806 post ray-finned fish duplicated genes, including *Neopterygii*, *Otophysa*, *Clupeocephala* and *Danio rerio* children taxa. We next removed duplicated genes that were found in common between the two

groups. This resulted in 8,601 pre-, and 3,249 post-ray-finned fish genes that we used in further analysis.

For the analysis of the expression pattern divergence, we focused on genes that were expressed in our data set. We analyzed expression pattern of all paralogs of DE genes (i.e. erythrocytes, monocytes, neutrophils, thrombocytes, HSPCs, NK- and T cells) that were expressed in more than 10% of cell in each of the branches (cell states). The expression pattern was considered to be conserved if duplicated genes and their annotated paralogs were all expressed in the same cell type. However, if at least one of the paralogs was expressed in a different cell type, this was considered as an example of potential functional divergence.

Deep Neural Network (DNN) Classifier

To generate the DNN model we used Keras[73], a Python based Deep Learning Library for Theano[74] and Tensorflow[75]. We worked with the Keras functional API, which allows the definition of complex systems, such as multi-output models.

The DNN was used to predict the probabilities of a specific Gene Expression profile to be classified into one of the four differentiated cell types. We used the entire set of genes for all differentiated cells in the branches (1,724 cells in total) i.e. erythrocytes, thrombocytes, neutrophils and monocytes. The input was therefore formed by 20,960 nodes (genes) which were normalized using z-values or standard scores. For the hyper-parametric fine tuning of the DNN, we generated and evaluated models with different number of hidden layers, hidden nodes, network initializations, regularizations and batch normalization. The final hyper parameters were chosen according to the optimal performance and convergence of the accuracy and loss values.

The model was comprised of 2 hidden layers with 100 and 50 nodes, using a weight decay regularisation with a λ-value of 0.001, and Gaussian Dropout of 0.8 between them. The chosen activation functions were ‘relu’ for the hidden layers, and ‘softmax’ for the output. The validation was performed over 20% of the initial dataset, using ‘categorical cross-entropy’ loss. The average classification accuracy after convergence was 0.998 ± 0.002, and cross entropy loss of 0.03± 0.004, validation accuracy of 0.964± 0.003 and cross entropy validation loss 0.15± 0.008.

The Neural Network output returns the probability of a Gene Expression input vector (cell) to be classified as each one of the differentiated cell types. We can use these probabilities and their distributions to generate a value that determines the "Stemness" of the cells according to the NN output. The "Stemness value" is a measure of similarity between the input vector and the average distributions for each output class, which can be then used to indicate the cell differentiation state of the input.

This measure has been previously[33] used for similar purposes. It is based on the Kullback-Leibler distance between probabilities, and the "Stemness value" (S_i) of cell "*i*" is determined by the equation:

$$S_i = \sum_{j=1}^{N_c} p_{ij} log \frac{p_{ij}}{\bar{p}_j}$$

Where N_c is the number of classes, and p_{ij} is the probability of cell *i* to belong to class *j*.

Cloud Repository

We have generated a cloud repository to enable research community to access single cell gene expression profiles of 1,422 zebrafish blood cells across all the 31,953 zebrafish genes. The implementation of the cloud service was performed using shiny[76] (version 0.14.2) https://shiny.rstudio.com, and plotly[77] (version 4.5.6) https://plot.ly R packages.

Statistics and reproducibility of experiments

Statistical tests were carried out using R software packages as indicated in the figure legends and the Methods section. No statistical method was used to predetermine sample sizes. Pearson Correlation Coefficient was used to compare the average profiles of single cells against the bulk. Significance of Differentially Expressed genes was calculated with an approximate likelihood ratio test (Monocle2 differentialGeneTest() function) of the full model "~state" cells against the reduced model "~1". For the Dynamically expressed genes, the full model "~sm.ns(Pseudotime)" was tested against the reduced model of no pseudotime dependence. In both cases, *P* values were normalised using the the Benjamini-Hochberg FDR (False Discovery Rate), selecting statistically significant genes with $P < 0.01$ and FDR < 0.1. For the GO analysis, the Hypergeometric Test (equivalent to the one tailed Fisher's exact test) was used to evaluate the significant terms, while *P* values were corrected for multiple testing using the FDR approach, with FDR < 0.05 considered statistically significant, using the gProfiler R[72] package.

DATA AVAILABILITY

Raw data can be found under the accession number E-MTAB-5530 on ArrayExpress (https://www.ebi.ac.uk/arrayexpress/). Additional Zebrafish related RNAseq data that were used in the present study can be found in E-MTAB-4617, E-MTAB-3947 while Human related data were collected from the Gene Expression Omnibus (GEO https://www.ncbi.nlm.nih.gov/geo/) under accession code GSE75478.

ACKNOWLEDGEMENTS

The study was supported by Cancer Research UK grant number C45041/A14953 (to A.C. and E.A.), European Research Council project 677501 – ZF_Blood (to A.C.) and a core support grant from the Wellcome Trust and MRC to the Wellcome Trust – Medical Research Council Cambridge Stem Cell Institute. The authors would like to thank WTSI Cytometry Core Facility for their help with index cell sorting and the Core Sanger Web Team for hosting the cloud web application. The authors would also like to thank the CRUK Cambridge Institute Genomics Core Facility for their contribution in sequencing the data.

AUTHOR CONTRIBUTIONS

E.I.A. carried out the analysis; J.G.B. and L.F. performed experiments; H.A. generated the DNN; P.L. oversaw implementation of the DNN; J.G.B., E.I.A., and A.C. contributed to the discussion of the results and designed figures; A.C. conceived the study and wrote the manuscript. All authors approved the final version of the manuscript.

COMPETING FINANCIAL INTERESTS

The authors declare no competing financial interests.

REFERENCES

1. Orkin, S. H. & Zon, L. I. Hematopoiesis: an evolving paradigm for stem cell biology. *Cell* **132,** 631–644 (2008).
2. Kondo, M., Weissman, I. L. & Akashi, K. Identification of clonogenic common lymphoid progenitors in mouse bone marrow. *Cell* **91,** 661–672 (1997).
3. Akashi, K., Traver, D., Miyamoto, T. & Weissman, I. L. A clonogenic common myeloid progenitor that gives rise to all myeloid lineages. *Nature* **404,** 193–197 (2000).
4. Adolfsson, J. *et al.* Identification of Flt3+ lympho-myeloid stem cells lacking erythro-megakaryocytic potential a revised road map for adult blood lineage commitment. *Cell* **121,** 295–306 (2005).
5. Månsson, R. *et al.* Molecular evidence for hierarchical transcriptional lineage priming in

fetal and adult stem cells and multipotent progenitors. *Immunity* **26,** 407–419 (2007).

6. Notta, F. *et al.* Distinct routes of lineage development reshape the human blood hierarchy across ontogeny. *Science* **351,** aab2116 (2016).
7. Spangrude, G. J., Heimfeld, S. & Weissman, I. L. Purification and characterization of mouse hematopoietic stem cells. *Science* **241,** 58–62 (1988).
8. Guo, G. *et al.* Mapping cellular hierarchy by single-cell analysis of the cell surface repertoire. *Cell Stem Cell* **13,** 492–505 (2013).
9. Wilson, N. K. *et al.* Combined Single-Cell Functional and Gene Expression Analysis Resolves Heterogeneity within Stem Cell Populations. *Cell Stem Cell* **16,** 712–724 (2015).
10. Jaitin, D. A. *et al.* Massively Parallel Single-Cell RNA-Seq for Marker-Free Decomposition of Tissues into Cell Types. *Science* **343,** 776–779 (2014).
11. Paul, F. *et al.* Transcriptional Heterogeneity and Lineage Commitment in Myeloid Progenitors. *Cell* **163,** 1663–1677 (2015).
12. Psaila, B. *et al.* Single-cell profiling of human megakaryocyte-erythroid progenitors identifies distinct megakaryocyte and erythroid differentiation pathways. *Genome Biol.* **17,** 83 (2016).
13. Yamamoto, R. *et al.* Clonal analysis unveils self-renewing lineage-restricted progenitors generated directly from hematopoietic stem cells. *Cell* **154,** 1112–1126 (2013).
14. Treutlein, B. *et al.* Reconstructing lineage hierarchies of the distal lung epithelium using single-cell RNA-seq. *Nature* **509,** 371–375 (2014).
15. Trapnell, C. *et al.* The dynamics and regulators of cell fate decisions are revealed by pseudotemporal ordering of single cells. *Nat. Biotechnol.* **32,** 381–386 (2014).
16. Macaulay, I. C. *et al.* Single-Cell RNA-Sequencing Reveals a Continuous Spectrum of Differentiation in Hematopoietic Cells. *Cell Rep.* **14,** 966–977 (2016).
17. Leng, L. *et al.* MIF signal transduction initiated by binding to CD74. *J. Exp. Med.* **197,** 1467–1476 (2003).
18. Shi, G. P. *et al.* Human cathepsin S: chromosomal localization, gene structure, and tissue distribution. *J. Biol. Chem.* **269,** 11530–11536 (1994).
19. Wittamer, V., Bertrand, J. Y., Gutschow, P. W. & Traver, D. Characterization of the mononuclear phagocyte system in zebrafish. *Blood* **117,** 7126–7135 (2011).
20. Furze, R. C. & Rankin, S. M. Neutrophil mobilization and clearance in the bone marrow. *Immunology* **125,** 281–288 (2008).
21. Rosowski, E. E., Deng, Q., Keller, N. P. & Huttenlocher, A. Rac2 Functions in Both Neutrophils and Macrophages To Mediate Motility and Host Defense in Larval Zebrafish. *J. Immunol.* **197,** 4780–4790 (2016).
22. Kumar, S. *et al.* Cdc42 regulates neutrophil migration via crosstalk between WASp,

CD11b, and microtubules. *Blood* **120,** 3563–3574 (2012).

23. Jones, R. A. *et al.* Modelling of human Wiskott–Aldrich syndrome protein mutants in zebrafish larvae using in vivo live imaging. *J. Cell Sci.* **126,** 4077–4084 (2013).
24. Grimm, T. *et al.* Dominant-negative Pes1 mutants inhibit ribosomal RNA processing and cell proliferation via incorporation into the PeBoW-complex. *Nucleic Acids Res.* **34,** 3030–3043 (2006).
25. Brombin, A., Joly, J.-S. & Jamen, F. New tricks for an old dog: ribosome biogenesis contributes to stem cell homeostasis. *Curr. Opin. Genet. Dev.* **34,** 61–70 (2015).
26. Ganis, J. J. *et al.* Zebrafish globin switching occurs in two developmental stages and is controlled by the LCR. *Dev. Biol.* **366,** 185–194 (2012).
27. Denker, B. M., Smith, B. L., Kuhajda, F. P. & Agre, P. Identification, purification, and partial characterization of a novel Mr 28,000 integral membrane protein from erythrocytes and renal tubules. *J. Biol. Chem.* **263,** 15634–15642 (1988).
28. Huang, H. & Cantor, A. B. Common features of megakaryocytes and hematopoietic stem cells: what's the connection? *J. Cell. Biochem.* **107,** 857–864 (2009).
29. Renshaw, S. A. *et al.* A transgenic zebrafish model of neutrophilic inflammation. *Blood* **108,** 3976–3978 (2006).
30. Long, Q. *et al.* GATA-1 expression pattern can be recapitulated in living transgenic zebrafish using GFP reporter gene. *Development* **124,** 4105–4111 (1997).
31. Tamplin, O. J. *et al.* Hematopoietic Stem Cell Arrival Triggers Dynamic Remodeling of the Perivascular Niche. *Cell* **160,** 241–252 (2015).
32. Tang, Q. *et al.* Optimized cell transplantation using adult rag2 mutant zebrafish. *Nat. Methods* **11,** 821–824 (2014).
33. Velten, L. *et al.* Human haematopoietic stem cell lineage commitment is a continuous process. *Nat. Cell Biol.* **19,** 271–281 (2017).
34. Ma, D., Zhang, J., Lin, H.-F., Italiano, J. & Handin, R. I. The identification and characterization of zebrafish hematopoietic stem cells. *Blood* **118,** 289–297 (2011).
35. Signer, R. A. J., Magee, J. A., Salic, A. & Morrison, S. J. Haematopoietic stem cells require a highly regulated protein synthesis rate. *Nature* **509,** 49–54 (2014).
36. Carroll, K. J. & North, T. E. Oceans of opportunity: exploring vertebrate hematopoiesis in zebrafish. *Exp. Hematol.* **42,** 684–696 (2014).
37. Carmona, S. J. *et al.* Single-cell transcriptome analysis of fish immune cells provides insight into the evolution of vertebrate immune cell types. *Genome Res.* **27,** 451–461 (2017).
38. Hakes, L., Pinney, J. W., Lovell, S. C., Oliver, S. G. & Robertson, D. L. All duplicates are not equal: the difference between small-scale and genome duplication. *Genome Biol.* **8,** R209 (2007).

39. Betancur-R., R. *et al.* The Tree of Life and a New Classification of Bony Fishes. *PLoS Curr.* (2013). doi:10.1371/currents.tol.53ba26640df0ccaee75bb165c8c26288
40. Watkins, N. A. *et al.* A HaemAtlas: characterizing gene expression in differentiated human blood cells. *Blood* **113,** e1–9 (2009).
41. Novershtern, N. *et al.* Densely interconnected transcriptional circuits control cell states in human hematopoiesis. *Cell* **144,** 296–309 (2011).
42. Chen, L. *et al.* Transcriptional diversity during lineage commitment of human blood progenitors. *Science* **345,** 1251033 (2014).
43. Nestorowa, S. *et al.* A single-cell resolution map of mouse hematopoietic stem and progenitor cell differentiation. *Blood* **128,** e20–31 (2016).
44. Lin, H.-F. *et al.* Analysis of thrombocyte development in CD41-GFP transgenic zebrafish. *Blood* **106,** 3803–3810 (2005).
45. Zhang, X. Y. & Rodaway, A. R. F. SCL-GFP transgenic zebrafish: in vivo imaging of blood and endothelial development and identification of the initial site of definitive hematopoiesis. *Dev. Biol.* **307,** 179–194 (2007).
46. Hall, C., Flores, M. V., Storm, T., Crosier, K. & Crosier, P. The zebrafish lysozyme C promoter drives myeloid-specific expression in transgenic fish. *BMC Dev. Biol.* **7,** 42 (2007).
47. Walton, E. M., Cronan, M. R., Beerman, R. W. & Tobin, D. M. The Macrophage-Specific Promoter mfap4 Allows Live, Long-Term Analysis of Macrophage Behavior during Mycobacterial Infection in Zebrafish. *PLoS One* **10,** e0138949 (2015).
48. Dee, C. T. *et al.* CD4-Transgenic Zebrafish Reveal Tissue-Resident Th2- and Regulatory T Cell-like Populations and Diverse Mononuclear Phagocytes. *J. Immunol.* **197,** 3520–3530 (2016).
49. Bielczyk-Maczyńska, E. *et al.* A Loss of Function Screen of Identified Genome-Wide Association Study Loci Reveals New Genes Controlling Hematopoiesis. *PLoS Genet.* **10,** e1004450 (2014).
50. Picelli, S. *et al.* Full-length RNA-seq from single cells using Smart-seq2. *Nat. Protoc.* **9,** 171–181 (2014).
51. Picelli, S. *et al.* Smart-seq2 for sensitive full-length transcriptome profiling in single cells. *Nat. Methods* **10,** 1096–1098 (2013).
52. Lee, H., Pine, P. S., McDaniel, J., Salit, M. & Oliver, B. External RNA Controls Consortium Beta Version Update. *J Genomics* **4,** 19–22 (2016).
53. Stachura, D. L. *et al.* Zebrafish kidney stromal cell lines support multilineage hematopoiesis. *Blood* **114,** 279–289 (2009).
54. Robert, C. & Watson, M. Errors in RNA-Seq quantification affect genes of relevance to human disease. *Genome Biol.* **16,** 177 (2015).

55. Dobin, A. *et al.* STAR: ultrafast universal RNA-seq aligner. *Bioinformatics* **29,** 15–21 (2013).
56. Kim, D. *et al.* TopHat2: accurate alignment of transcriptomes in the presence of insertions, deletions and gene fusions. *Genome Biol.* **14,** R36 (2013).
57. Langmead, B. & Salzberg, S. L. Fast gapped-read alignment with Bowtie 2. *Nat. Methods* **9,** 357–359 (2012).
58. Patro, R., Duggal, G., Love, M. I., Irizarry, R. A. & Kingsford, C. Salmon provides fast and bias-aware quantification of transcript expression. *Nat. Methods* **14,** 417–419 (2017).
59. Patro, R., Mount, S. M. & Kingsford, C. Sailfish enables alignment-free isoform quantification from RNA-seq reads using lightweight algorithms. *Nat. Biotechnol.* **32,** 462–464 (2014).
60. Bray, N. L., Pimentel, H., Melsted, P. & Pachter, L. Near-optimal probabilistic RNA-seq quantification. *Nat. Biotechnol.* **34,** 525–527 (2016).
61. Anders, S., Pyl, P. T. & Huber, W. HTSeq--a Python framework to work with high-throughput sequencing data. *Bioinformatics* **31,** 166–169 (2015).
62. Trapnell, C. *et al.* Transcript assembly and quantification by RNA-Seq reveals unannotated transcripts and isoform switching during cell differentiation. *Nat. Biotechnol.* **28,** 511–515 (2010).
63. L. Lun, A. T., Bach, K. & Marioni, J. C. Pooling across cells to normalize single-cell RNA sequencing data with many zero counts. *Genome Biol.* **17,** 75 (2016).
64. Brennecke, P. *et al.* Accounting for technical noise in single-cell RNA-seq experiments. *Nat. Methods* **10,** 1093–1095 (2013).
65. Buettner, F. *et al.* Computational analysis of cell-to-cell heterogeneity in single-cell RNA-sequencing data reveals hidden subpopulations of cells. *Nat. Biotechnol.* **33,** 155–160 (2015).
66. Stacklies, W., Redestig, H., Scholz, M., Walther, D. & Selbig, J. pcaMethods--a bioconductor package providing PCA methods for incomplete data. *Bioinformatics* **23,** 1164–1167 (2007).
67. Marchini, J. L., Heaton, C., Ripley, M. B. & Suggests, M. Package 'fastICA'. (2017).
68. Haghverdi, L., Buettner, F. & Theis, F. J. Diffusion maps for high-dimensional single-cell analysis of differentiation data. *Bioinformatics* **31,** 2989–2998 (2015).
69. Maechler, M., Rousseeuw, P., Struyf, A. & Hubert, M. 2005. cluster: Cluster Analysis Basics and Extensions.
70. Wickham, H. *ggplot2: Elegant Graphics for Data Analysis*. (Springer New York, 2009).
71. Kolde, R. Pheatmap: pretty heatmaps. *R package version* **61,** (2012).
72. Reimand, J. *et al.* g:Profiler-a web server for functional interpretation of gene lists (2016

update). *Nucleic Acids Res.* **44,** W83–9 (2016).

73. Chollet, F. & Others. Keras. (2015).
74. Al-Rfou, R. *et al.* Theano: A Python framework for fast computation of mathematical expressions. *arXiv e-prints* **abs/1605.02688,** (2016).
75. Allaire, J. J., Eddelbuettel, D., Golding, N. & Tang, Y. tensorflow: R Interface to TensorFlow. (2016).
76. Chang, W., Cheng, J., Allaire, J. J., Xie, Y. & McPherson, J. shiny: Web Application Framework for R. (2017).
77. Sievert, C. *et al.* plotly: Create Interactive Web Graphics via 'plotly.js'. (2017).

FIGURE LEGENDS

Figure 1. Pseudotime ordering reveals a gradual transition of cells from immature to more differentiated within the myeloid branch

a) Experimental strategy for sorting single cells from transgenic zebrafish lines. Cells were harvested from a single kidney of each line and sorted for expression of the fluorescent transgene. Index sorting was used to dispense single cells into a 96 well plate and these were subsequently processed for RNA-seq analyses. b) Five cell states were predicted using the Monocle2 algorithm for temporal analyses of single cell transcriptomes. c) Analysis of genes that are differentially expressed across the five states (given the same colour code used in b) reveals GO terms (inner circle) that are highly pertinent to specific cell types. The outer circle shows examples of May-Grünwald Giemsa stained cells from kidneys of transgenic lines that largely label each particular cell type. d) Jitter plots showing the expression (y axis) of differentially expressed marker genes in each cell type (x axis). Each dot in the jitter plot shows the expression of the gene $\log_{10}$ (counts + 1) in each cell.

Figure 2. The distribution of cells from different transgenic lines modelled by Monocle

a) The trajectories of cell states predicted by Monocle are shown in grey for each transgenic line used, with the associated cell types labelled in blue. The percentage of cells from each transgenic line contributing to each state is given next to the relevant trajectory. b) Pie charts showing the contribution of transgenic lines to each cell type. The colour code relates to the colours given in the headers for each transgenic line used in (a).

Figure 3. Cells within distinct states have different repopulation potentials

a) Experimental strategy for the adult transplantation experiment. Kidneys were dissected from transgenic donor fish and sorted for cells expressing the fluorescent transgene. Positive cells were collected and injected into sub-lethally irradiated *rag2*$^{E450fs-/-}$ fish. b) Assessment

for engraftment was made one day, four- and 14 weeks post transplantation using flow cytometry. Successfully engrafted fluorescent donor cells were isolated at four weeks PI by index sorting single cells into a microtitre plate for subsequent RNA-seq analyses. c) Distribution of *runx1*+ cells, from non-transplanted (left) and transplanted fish at 4 (middle) and 14 wpt (right), modelled by Monocle.

Figure 4. Transcriptionally similar cells display different probabilities of being stem cells. a) Cells predicted to be stem cells in the middle part of the lineage tree according to their stemness index. The insert shows the new Monocle tree including transplanted cells (1,724 single cells and 1,871 highly variable genes). b) Distribution of stemness scores in different branches of the tree showing the presence of potential HSCs exclusively in the HSPC branch. c) Contribution of different transgenic lines to predicted stem cells.

Figure 5. Lineage differentiation is defined by two main trends in gene expression
a) Heatmap of genes whose expression changed dynamically during pseudotime in each of the four branches. b) Graph showing the average expression pattern of the dynamically expressed genes that follow the same trend across pseudotime. For each of the cell states, one gene is presented that follows one of the two main trends. Standard error is shown as a gray area around the trend lines. c) Heatmap of expression of 168 genes annotated as “ribosomal proteins” genes in pseudotime in each of the four branches.

Figure 6. Conservation analysis of zebrafish genes differentially expressed in the main blood cell types.
a) Percentage of zebrafish protein-coding genes (specific for distinct blood cell types, as well as non-differentially expressed) with orthologs in other vertebrate species. b) The total number of paralogs duplicated exclusively pre- (green) and post ray-finned speciation (red). The numbers 1-7 mark the number of cell types (erythrocytes, monocytes, neutrophils, thrombocytes, HSPCs, T-cells and NK cells) in which the duplicated genes are expressed. c) The percentage of conserved vs diverged genes duplicated exclusively post speciation (fish specific genes).

Supplementary Figure 1. Comparison of the difference between unique and multi-mapped alignment methods on our scRNA-Seq data set. a) Pearson correlation of the average gene expressions between Salmon and Sailfish. Gene quantification accuracy was assessed by selecting for each of the 21 sequenced plates the average $\log_{10}$ (TPM+1) gene expressions. b) Violin plots of the number of detected genes (TPM>1) at single-cell level. Salmon (unique mapped reads) and Sailfish (multi-mapped reads) were compared for each

of the 21 plates. c) Distribution of the Coefficient of Variation. Comparison of log10(CV+0.001) gene expression (TPMs) values at a single-cell level between Salmon (unique mapped reads) and Sailfish (multi-mapped reads), across 21 plates.

Supplementary Figure 2. Quality control of scRNA-seq data

Plots for the number of input reads, detected genes, %ERCCs and % mitochondrial (MT) genes on the y-axis in columns versus these four parameters on the x-axis in rows. The key in the bottom right hand plot indicates cells that have passed the quality control (% ERCCs <60%, mt <60%, at least 1000 detected genes), those that have failed and controls (bulk cells, empty wells and testes).

Supplementary Figure 3. Quality control of scRNA-seq data in the erythroid lineage and comparison of bulk versus single cell transcriptomes

The expression of the erythroid specific genes *ba1* and *hbaa1* were taken into account for quality control. a) and (c) plots show that many of the cells that initially failed QC (see key in a) have high expression of *ba1* (a) and *hbaa1* (c). These cells were therefore reassessed and those with >40000 *ba1* TPM (B) or >9000 *hbaa1* TPM (d) were included in the dataset. e) Correlation of average single cell transcriptome profiles and corresponding bulk wells for each fish line. The Pearson correlation coefficient shown in each plot indicates a strong correlation (0.7-0.9) between single and bulk transcriptome profiles.

Supplementary Figure 4. Representation of single cell transcriptomes in three dimensional component space and the identification of the most highly variable genes

a) The 1,845 most highly variable genes were used to generate a diffusion map, independent component analyses and principal component analyses. The approximate positions of the cell states identified by Monocle 2 (Figure 1) are shown in the insert. Cells were derived from the transgenic lines and plates as listed in the key. b) The graph shows the squared coefficient of variance (CV^2) plotted versus mean read counts. The solid magenta line shows the curve of the technical noise fit and the dashed yellow line shows the position of genes with 25% biological CV. Blue dots indicate the ERCCs; magenta dots indicate the significantly variable genes; brown dots show the rest of genes expressed in the dataset.

Supplementary Figure 5. Monocle trajectories generated using different sets of highly variable genes. Trajectories were generated using three different sets of highly variable genes. Highly variable genes were calculated using thresholds of 5%, 25%-(default) and

95% biological variation. For each reconstructed tree, the percentage (and a total number) of "misclassified" cells in each branch was calculated compared to the default setup (25%). k=number of components used.

Supplementary Figure 6. The isolation and morphological characterisation of transgenic cell types

Representative FACS plots of cells isolated for scRNA-seq from each transgenic line. All cells that were positive for the fluorescent transgene were plotted on to forward/side scatter plots of live cells and are shown as coloured dots. To the right of each plot are the names of the genes and representative cells that were isolated by cytospins and stained with May-Grünwald Giemsa.

Supplementary Figure 7. The morphological characteristics of wild type cell sub-populations and their distribution in Monocle2

a**)** Flow cytometry forward scatter/side scatter plot of the wild type whole kidney marrow, showing the gating strategy for isolating populations P1-5. The percentage of live cells in each gate is also given. The cells on the left hand side of the P1 and P2 were gated out because the majority of these cells are erythrocytes. b) The cytospins of the representative cells from P1-P5 stained with May-Grünwald Giemsa. c) The trajectories of cell states predicted by Monocle are shown in grey for P1-P5, with the associated cell types labelled in blue. The percentage of cells from each sub-population contributing to each state is given next to the relevant trajectory.

Supplementary Figure 8. Correlation analysis between ribosomal and cell cycle related genes. (a) Correlation heatmaps across all ribosomal and cell cycle genes, (b) correlation heatmaps of ribosomal and cell cycle genes in pseudotime and (c) average expression patterns of ribosomal and cell cycle genes in pseudotime.

Supplementary Figure 9. Analysis of ribosomal genes in human HSCs and progenitors. a) Heatmap of ribosomal gene expression in human HSCs and progenitors. Clustering of all human ribosomal genes across different HSPC populations, using Euclidean distance and Ward Linkage. b) Correlation analysis of expressed ribosomal genes across 891 HSPCs. Pairwise Pearson correlation revealed similar expression levels of the expressed cytosolic ribosomal genes in HSC and various progenitors (MPP, CMP, GMP, MEP and MLP).

Supplementary Table 1. Details of transgenic and wild type lines used for single cell experiments, giving age, number of fish, number of 96 well plates sorted, number of cells passing quality control and references.

Supplementary Table 2. Full list of the DE expressed genes in each of the five Monocle states; GO term enrichment analysis for each of the states; dynamically expressed genes in monocytes, neutrophils, erythrocytes and thrombocytes; expression of ribosomal genes which show dynamic and random expression in pseudotime in monocytes, neutrophils, erythrocytes and thrombocytes.

Supplementary Table 3. Detailed description of the Human progenitor populations considered in the present study with their respective FACS markers.

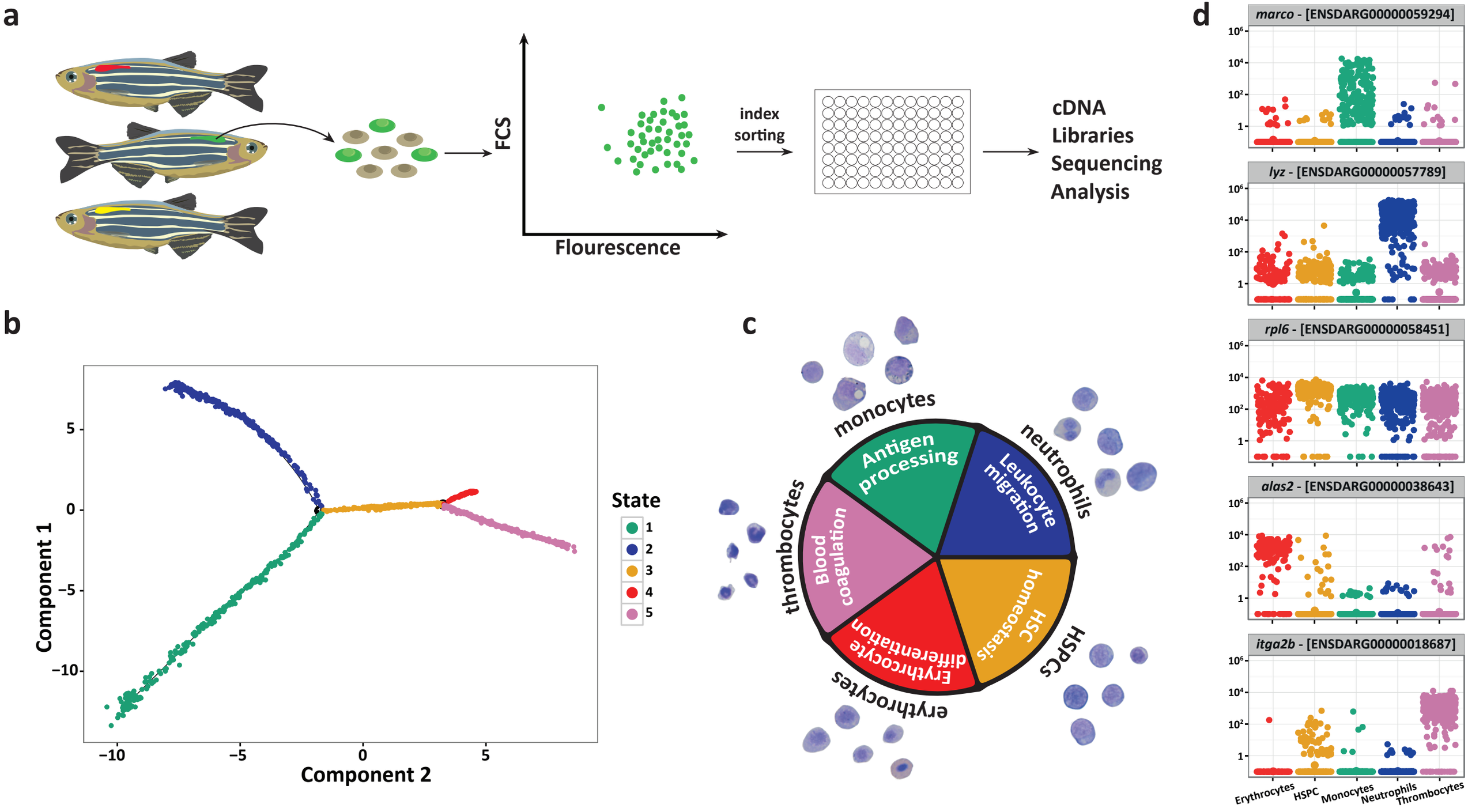
a
FCS
Flourescence
index
sorting
cDNA
Libraries
Sequencing
Analysis
b
Component 1
Component 2
State
1
2
3
4
5
c
monocytes
neutrophils
HSPCs
erythrocytes
thrombocytes
Antigen processing
Leukocyte migration
HSC homeostasis
Erythrocyte differentiation
Blood coagulation
d
marco - [ENSDARG00000059294]
lyz - [ENSDARG00000057789]
rpl6 - [ENSDARG00000058451]
alas2 - [ENSDARG00000038643]
itga2b - [ENSDARG00000018687]
Erythrocytes
HSPC
Monocytes
Neutrophils
Thrombocytes

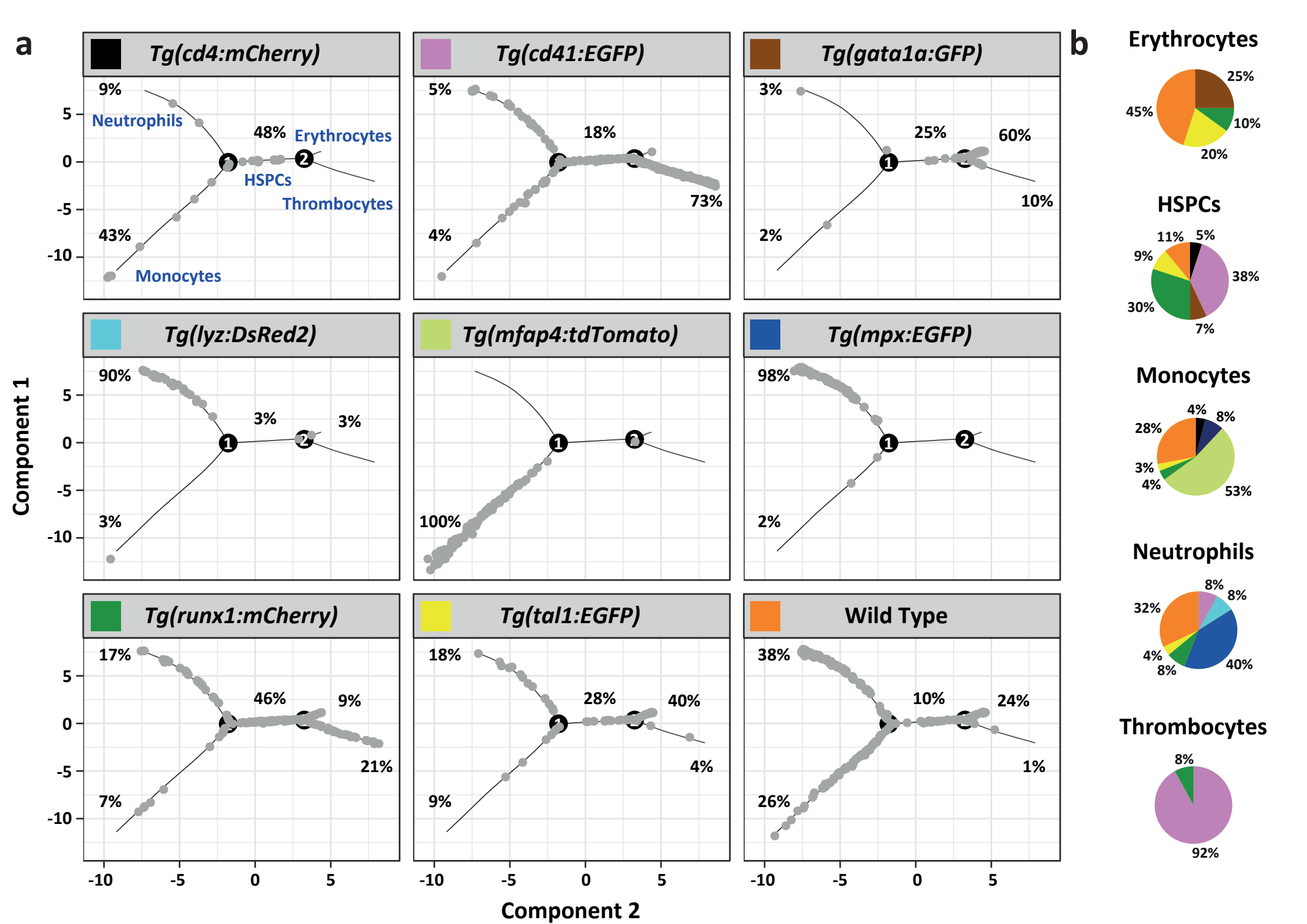
a
Tg(cd4:mCherry)
9%
Neutrophils
48%
Erythrocytes
HSPCs
Thrombocytes
43%
Monocytes
Tg(cd41:EGFP)
5%
18%
73%
4%
Tg(gata1a:GFP)
3%
25%
60%
10%
2%
Tg(lyz:DsRed2)
90%
3%
3%
3%
Tg(mfap4:tdTomato)
100%
Tg(mpx:EGFP)
98%
2%
Tg(runx1:mCherry)
17%
46%
9%
21%
7%
Tg(tal1:EGFP)
18%
28%
40%
4%
9%
Wild Type
38%
10%
24%
1%
26%
Component 1
Component 2
-10
-5
0
5
b
Erythrocytes
25%
45%
10%
20%
HSPCs
11%
5%
9%
38%
30%
7%
Monocytes
4%
8%
28%
3%
4%
53%
Neutrophils
8%
8%
32%
4%
8%
40%
Thrombocytes
8%
92%

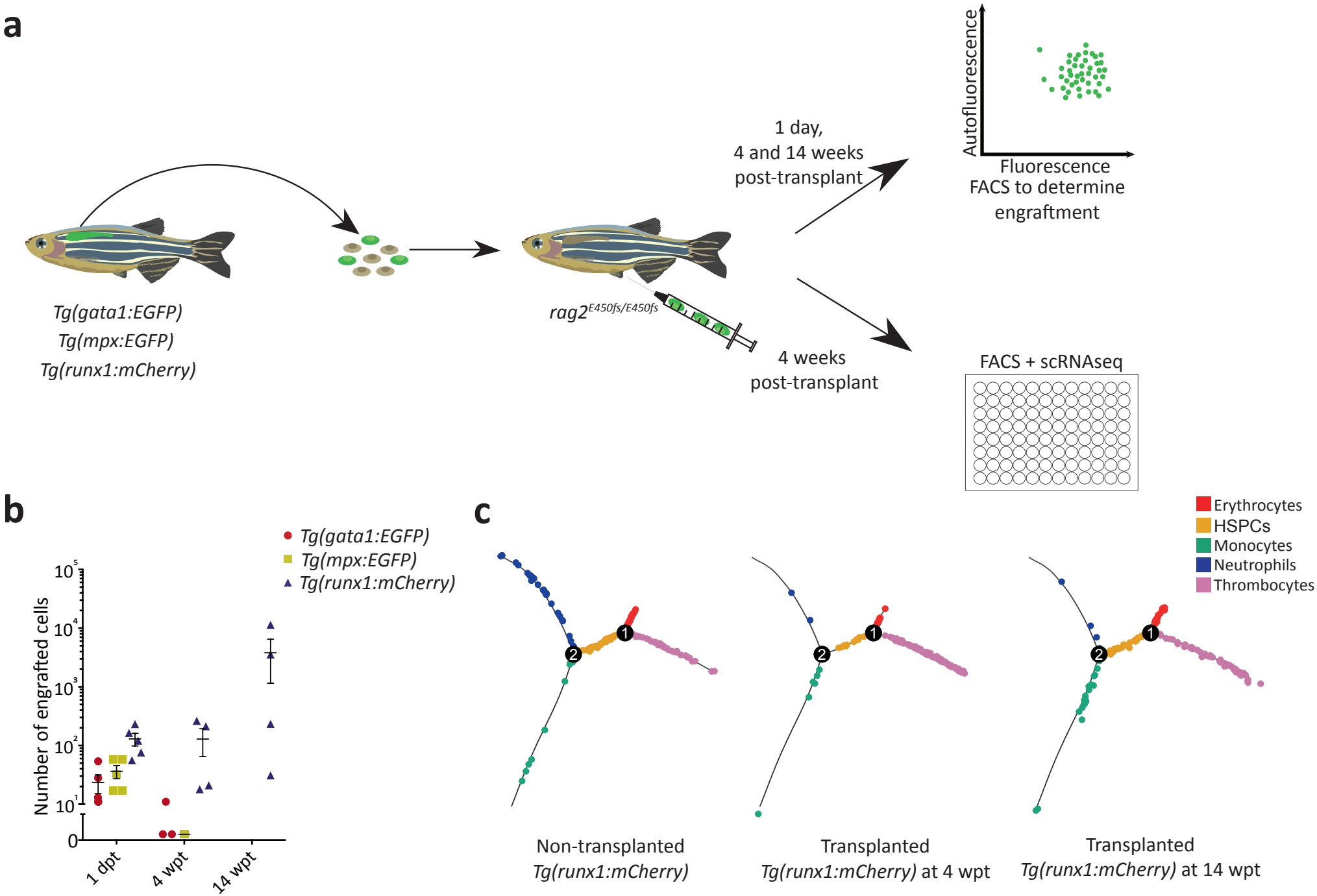
a
Tg(gata1:EGFP)
Tg(mpx:EGFP)
Tg(runx1:mCherry)
rag2E450fs/E450fs
1 day,
4 and 14 weeks
post-transplant
Autofluorescence
Fluorescence
FACS to determine
engraftment
4 weeks
post-transplant
FACS + scRNAseq
b
Tg(gata1:EGFP)
Tg(mpx:EGFP)
Tg(runx1:mCherry)
Number of engrafted cells
1 dpt
4 wpt
14 wpt
c
Erythrocytes
HSPCs
Monocytes
Neutrophils
Thrombocytes
Non-transplanted
Tg(runx1:mCherry)
Transplanted
Tg(runx1:mCherry) at 4 wpt
Transplanted
Tg(runx1:mCherry) at 14 wpt

a

b

c

Erythrocytes

Monocytes

Neutrophils

Thrombocytes

ba1

marco

mpx

itga2b

rpl14

rpl6

rps3a

rpl3

Genes

$\log_{10}$(Counts+1)

Cytosolic

Mitochondrial

Pseudotime

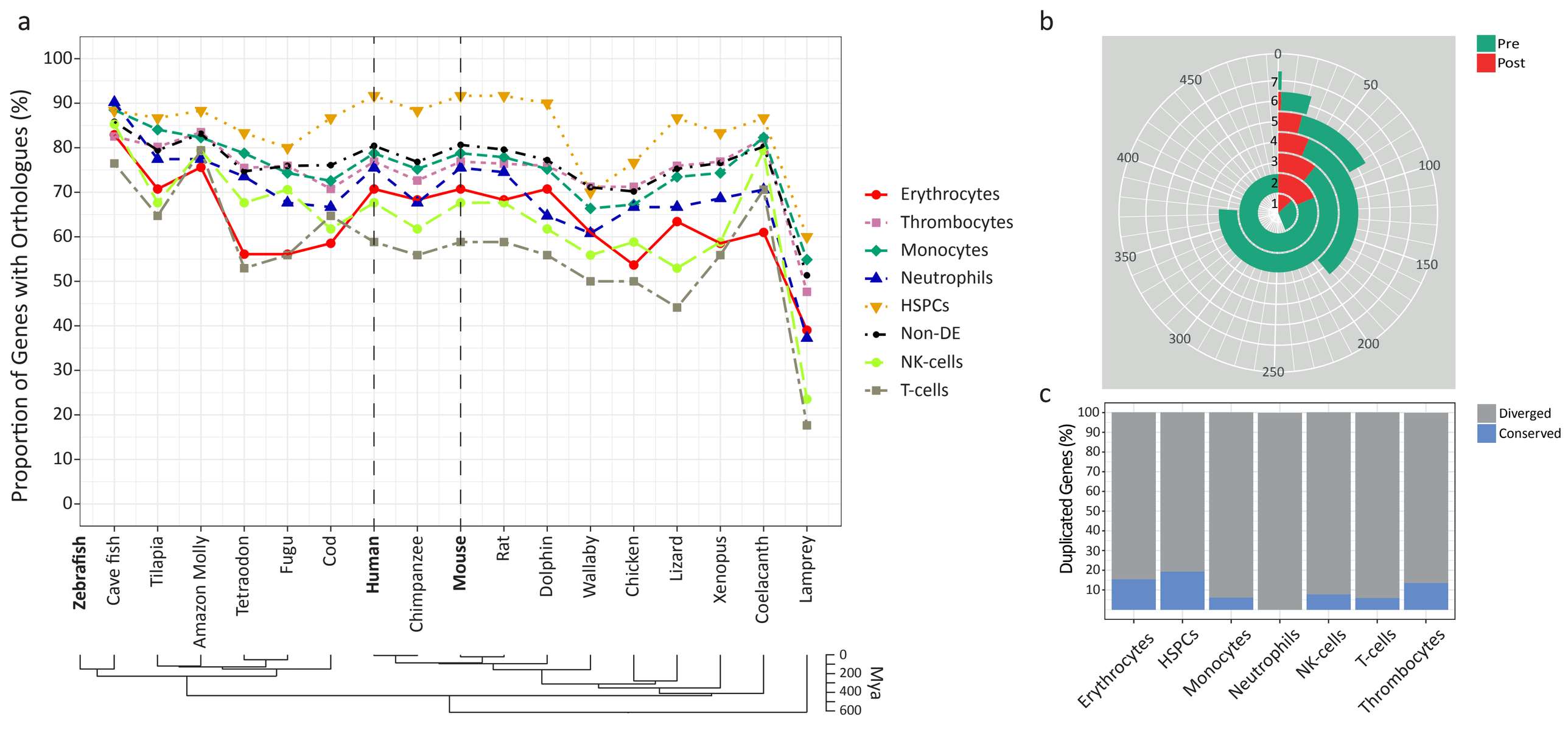
a
Proportion of Genes with Orthologues (%)
100
90
80
70
60
50
40
30
20
10
0
Erythrocytes
Thrombocytes
Monocytes
Neutrophils
HSPCs
Non-DE
NK-cells
T-cells
Zebrafish
Cave fish
Tilapia
Amazon Molly
Tetraodon
Fugu
Cod
Human
Chimpanzee
Mouse
Rat
Dolphin
Wallaby
Chicken
Lizard
Xenopus
Coelacanth
Lamprey
0
200
400
600
Mya
b
Pre
Post
0
50
100
150
200
250
300
350
400
450
1
2
3
4
5
6
7
c
Duplicated Genes (%)
100
90
80
70
60
50
40
30
20
10
Diverged
Conserved
Erythrocytes
HSPCs
Monocytes
Neutrophils
NK-cells
T-cells
Thrombocytes